Carbohydrate Research 432 (2016) 9–16

Contents lists available at ScienceDirect

Carbohydrate Research

journal homepage: www.elsevier.com/locate/carres

A one-pot synthesis of 1,6,9,13-tetraoxadispiro(4.2.4.2)tetradecane by hydrodeoxygenation of xylose using a palladium catalyst☆

Michael A. Jackson [a, *], Judith A. Blackburn [a], Neil P.J. Price [a], Karl E. Vermillion [b], Steven C. Peterson [c], Gregory M. Ferrence [d]

[a] United States Department of Agriculture, Agricultural Research Service, National Center for Agricultural Utilization Research, Renewable Products Technology Research, 815 N. University, St. Peoria, IL 61604, United States
[b] United States Department of Agriculture, Agricultural Research Service, National Center for Agricultural Utilization Research, Functional Foods Research, 815 N. University, St. Peoria, IL 61604, United States
[c] United States Department of Agriculture, Agricultural Research Service, National Center for Agricultural Utilization Research, Plant Polymer Research, 1815 N. University, St. Peoria, IL 61604, United States
[d] Department of Chemistry, Illinois State University, Normal, IL 61790, United States

ARTICLE INFO

Article history:
Received 26 May 2016
Accepted 9 June 2016
Available online 14 June 2016

Keywords:
Xylose
Arabinose
Pd/silica-alumina
Polymorph
1,6,9,13-tetraoxadispiro(4.2.4.2)tetradecane
11β-hydroxysteroid dehydrogenase 1

ABSTRACT

In an effort to expand the number of biobased chemicals available from sugars, xylose has been converted to 1,6,9,13-tetraoxadispiro(4.2.4.2)tetradecane in a one-pot reaction using palladium supported on silica-alumina as the catalyst. The title compound is produced in 35–40% yield under 7 MPa H_2 pressure at 733 K using 3–10 wt%Pd on silica-alumina catalyst. It is isolated using a combination of liquid-liquid extractions and flash chromatography. This dimer can be converted to its monomer, 2-hydroxy-(2-hydroxymethyl)tetrahydrofuran, which ring opens under acid conditions to 1,5-dihydroxy-2-pentanone. This diol can then be esterified with vinylacetate in phosphate buffer to produce 1,5-bis(acetyloxy)-2-pentanone which is an inhibitor of mammalian 11β-hydroxysteroid dehydrogenase 1. ^{1}H and ^{13}C nmr spectra of each of these species are reported. The single crystal X-ray structure of the title compound is also reported. These data were collected in a temperature range of 100 K–273 K and show a solid state phase change from triclinic to monoclinic between 175 K and 220 K without a conformational change.

Published by Elsevier Ltd.

1. Introduction

Xylose is a readily available pentose usually isolated from the hemicellulose of wood, typically, beech and birch. Much of the commercial use of xylose is in its hydrogenation to xylitol [1,2]. In 2013 xylitol had a global market value of US$670 million [3] that is expected to grow to US$1 billion by 2020. The hydrogenation is performed using Raney nickel in a batch slurry reactor where the catalyst effectively hydrogenates the carbonyl group of xylose. However, the utilization of xylose in a biobased chemicals program requires xylose to be converted to a wide spectrum of chemicals. Extensive research exists into the dehydration of xylose to make furfural which can then be a building block used in many industries [4–12]. The hydrogenation of furfural yields biofuel components [13–18] and diol monomers [19–22] for polymer synthesis. Other specialty products have been prepared from the pentoses. van der Klis et al. have reported on the decarbonylation of xylose and arabinose over Ru/C to give the tetritols erythritol and threitol at 25% yield [23].

We present here another specialty product from xylose, 1,6,9,13-tetraoxadispiro(4.2.4.2)tetradecane, (**1**), which was originally described simultaneously by Hurd [24] and Swadesh [25] in 1949. Hurd was attempting to resolve discrepancies previously reported on the thermal degradation of sugars. He used 2,3-dihydroxytetrahydropyran as a model compound for studying the degradation of glucose but failed to find the expected anhydroglucose analog. Instead, **1** was found in about 20% yield. Swadesh, while at Quaker Oats, was identifying the byproducts resulting from the Raney nickel hydrogenation of furfuryl alcohol

☆ Mention of trade names or commercial products in this publication is solely for the purpose of providing specific information and does not imply recommendation or endorsement by the U.S. Department of Agriculture. USDA is an equal opportunity provider and employer.

* Corresponding author.
E-mail address: michael.jackson@ars.usda.gov (M.A. Jackson).

http://dx.doi.org/10.1016/j.carres.2016.06.003
0008-6215/Published by Elsevier Ltd.

where tetrahydrofurfurylalcohol is the main product. One of the byproducts, described as high-boiling, was isolated as a colorless crystal melting at 103 °C. Following discussions between Swadesh and Hurd, it was concluded that each group was studying the same compound, namely **1**. After a fifty year absence from the literature, the structure of **1** was determined by Gaede et al. [26] This group used a Pd/C catalyst for the hydrogenation of furfuryl alcohol and recovered **1** at a yield of less than 5%. They found the product deposited in the condenser while attempting a distillation. Each of these groups also noted the monomeric, ring-opened form of the compound, 1,5-dihydroxy-2-pentanone. More recently, Zhang, et al. [27] isolated **1** and several derivatives including the mono- and diacetylated derivatives of 1,5,-dihydroxy-2-pentanone from the fruiting spores of the basidiomycete *Catathalesma imperial*. The compounds were isolated by ethyl acetate extraction and purified by column chromatography in quantities ranging from 2 to 110 mg/kg of fungal fruiting tissue. Three of these isolated compounds in open chain form, though not the cyclic species, were found to be inhibitors of both human and mouse 11β-hydroxysteroid dehydrogenases. These enzymes are seen as targets for treating hypertension, type II diabetes, and metabolic syndrome [28]. This report offers some expectation for the utility of **1**, either as the tricyclic or its open chain form.

We rediscovered the title compound while screening catalysts for the hydrodeoxygenation of biomass hydrolysates. The hydrolysates were prepared by passing hot, compressed water over ball-milled switchgrass. These screening reactions were performed on these murky suspensions at 433 K and 7 MPa hydrogen pressure and resulted in solutions containing products from both lignin and sugar components of biomass. Analysis of these solutions by gas chromatography/mass spectrometry and HSQC NMR led to the tentative identification of **1**. The structure of **1** suggested that it originated with xylose and/or arabinose that were hydrolyzed from hemicellulose. Therefore, these pentoses were hydrogenated under the conditions of our screening reactions to see if **1** could be synthesized in high yields and to see if it could serve as biobased platform chemical. The results of these studies are presented here.

2. Results and discussion

2.1. Catalyst selection and characterization

From our screening reactions it was apparent that palladium was the active metal with the greatest tendency to produce **1** from xylose and it performed best when supported on silica-alumina (SA). Other supports that were examined included commercial 5% $Pd/CaCO_3$, 5%Pd/C, and 5%Pd/Al_2O_3. Of these, only the 5%Pd/Al_2O_3 gave **1** in yields near that obtained with Pd/SA. 5%Pd/C gave **1** at <5% and xylitol and tetrahydrofurfuryl alcohol (THFA) at selectivities of 35% and 41%, respectively. 5%$Pd/CaCO_3$ produced mostly the hydrogenolysis products acetol, 3-hydroxy-2-butanone, and acetic acid and **1** at only 6%. Palladium was also impregnated onto other supports. 5%$Pd/AlPO_4$ was prepared to examine the role support acidity might play. This catalyst did produce **1** at 12% selectivity (and THFA at 38%) but it was visibly degraded after one use. Palladium was loaded onto H-Beta zeolite, another acidic support, which gave **1** at 20% yield along with THFA and acetol. Following these results, we focused on the Pd/SA catalysts for the synthesis of **1**.

A series of Pd/SA catalysts with Pd loadings ranging from 3% to 10% were prepared by wet impregnation using $PdCl_2$ dissolved in aqueous ammonium hydroxide. The surface properties of fresh and used 5Pd/SA catalysts calcined at 673–973 K are shown in Table 1 and the N_2 isotherms of the catalyst calcined at 973 K are shown in Fig. 1. It can be seen in the table that addition of the palladium to the support causes a decrease in surface area and small changes in pore diameter and volume. Calcination at 973 K causes a greater loss in surface area compared to the lower temperatures. PdO crystallite size is also affected by calcination temperature with the higher temperatures giving larger crystallites. Metal oxide supports are known to be susceptible to degradation in hot water and this can be seen in both the table and in the shape of the N_2 isotherms. The loss in surface area and expansion of the pores reveals the change in the support structure. Fig. 1 shows the hysteresis loop of the fresh catalyst is a Type H2 typical of metal oxide gels and indicative of complex, interconnected pore structure. After use, the pore structure appears to collapse into fewer but larger pores resulting in a hysteresis loop that takes on the appearance of Type H1. This reorganization also affects the PdO crystallite size as the X-ray diffraction results from the fresh and used catalysts indicate that the crystallites are smaller after the catalysts have been used. The energy dispersive X-ray spectroscopic analysis of Pd and Al also indicate that the Pd migrates to the surface as a result of both calcination temperature and use. Overall, this means that the calcination temperature becomes irrelevant after the catalysts are exposed to hot water. (See the SI for the XRD and EDS spectra in Figs. S1 and S3).

Fig. S2 displays the temperature programmed hydrogenation of the catalysts after being calcined at temperatures of 673 K, 773 K, and 973 K. The negative peak, an area where hydrogen is being evolved from the catalyst, is indicative of the β-hydride capacity of the reduced Pd^0 on the surface of the catalyst. The TPR trace of the catalyst calcined at 673 K shows a smaller negative peak at 358 K and a large hydrogen absorption peak near 573 K. The peak around 573 K results from better dispersed Pd on the surface. At higher calcination temperatures, the β-hydride peak increases in size and the dispersed Pd is reduced in relative amounts.

2.2. Hydrodeoxygenation of D-(+)-xylose

The title compound is a colorless solid with a literature melting point of 376 K; at high purity, it sublimes; it has a fragrance variously described as like that of hazelnut or bourbon. The hydrodeoxygenation (HDO) of xylose to **1** and the successive conversion of this to the ring-opened species 1,5-dihydroxy-2-pentanone (**3**) and on to the acetylated derivative (**4**) are shown in Fig. 2. The yield-limiting step in the reaction series is the reaction of xylose with a yield of **1** typically at 35–40%. Fig. 3 displays the product selectivity at high conversion of xylose. The identified side products of this reaction result from as many as four competing pathways that need to be inhibited to increase the yield of **1**. These include hydrogenolysis in which carbon-carbon bonds are broken giving hydroxypropanone and 1-hydroxy-2-butanone. The second pathway is the HDO of xylose in which carbon-oxygen bonds are broken resulting in the formation of water and the C5 products 1-hydroxy-2-pentanone, cyclopentanone, and THFA. The third pathway is the hydrogenation of the carbonyl group to give xylitol. A fourth pathway is the dehydration of xylose to furfural, which is a well known route to platform chemicals from biomass [4–7,9,29]. But furfural is only detected at very low levels during the HDO reaction. Although furfural could be seen as the logical precursor to **1** if it was hydrogenated to furfuryl alcohol, the starting material in the previous reports for the synthesis of **1**. In fact, the hydrogenation of furfuryl alcohol over Pd/SA does not give **1**. Furfural could also be proposed as the precursor to both THFA [13] and the cyclopentanone [30,31]. The hydrogenation of furfural proceeds only slightly under these reaction conditions over Pd/SA so the THFA likely forms from the HDO pathway. Furfural is not formed if the catalyst is more active toward the reactions involving hydrogen than toward dehydration. That is, palladium catalysts activate hydrogen and produce the reduced organic species. Other

Table 1
Textural properties of the catalyst calcined at various temperatures, fresh, and after use.

Catalyst (calcination temperature, K)	BET SA, m^2/g	d_p, nm	Pore vol. cm^3/gr	PdO size by XRD, nm	wt%Pd by EDS	wt%Al by EDS
Silica-alumina(973)	554	4.1	0.65	–	–	8.92
5Pd/SA(673)	484	5.4	0.59	14.4	10.53	6.77
5Pd/SA(673) used	306	11.1	0.67	12.3	7.61	6.65
5Pd/SA(773)	497	4.2	0.58	14.7	7.57	6.42
5Pd/SA(773) used	289	11.1	0.61	12.9	8.19	8.60
5Pd/SA(973)	370	5.4	0.47	22.1	8.36	7.20
5Pd/SA(973) used	286	9.9	0.56	12.8	10.89	6.73

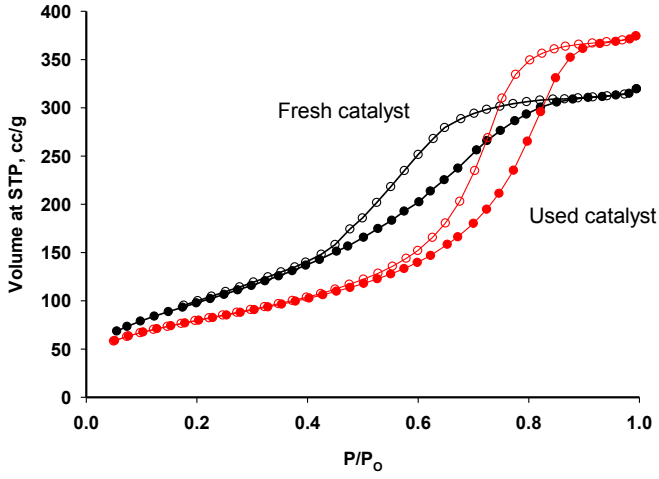

Fig. 1. N_2 isotherms of fresh and used 5%Pd/SA(973) showing the change in surface texture of the catalyst after one run.

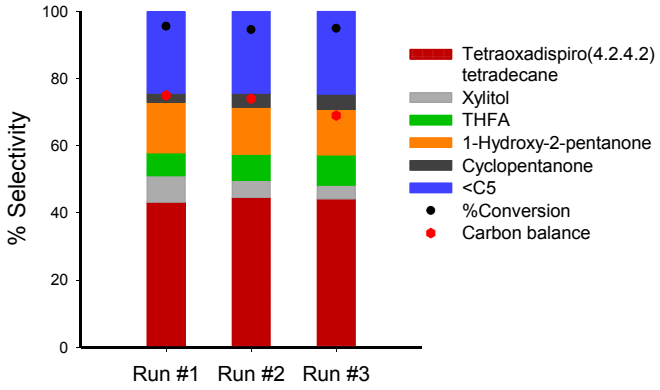

Fig. 3. Product distribution from repeated runs with the 5%Pd/SA catalyst.

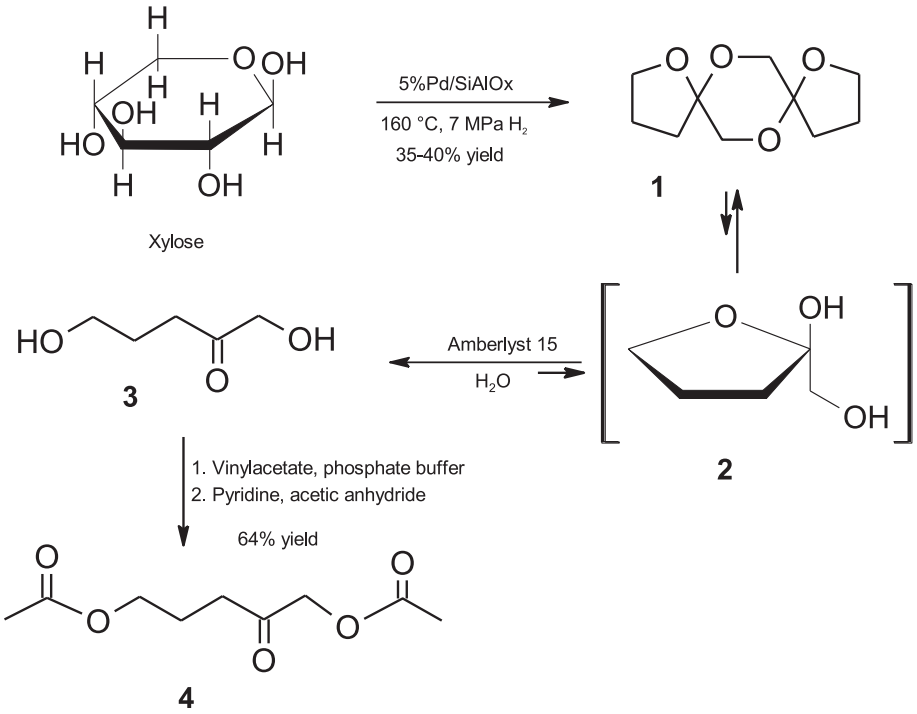

Fig. 2. Scheme showing the conversions from xylose to 1,5-bis(acetyloxy)-2-pentanone.

hydrogenation catalysts that were screened, including Pt, Cu, Ni, and Rh, on silica-alumina, gave enough furfural for the formation of oligomeric furfural humins to be visible in the reactor as tars. Only the Rh/SA gave **1** in appreciable yield.

2.3. Effect of reaction conditions on yield

2.3.1. Effect of hydrogen pressure

Yields of **1** were greatly improved by increased hydrogen pressure. When the hydrogenation of 5% xylose solutions was performed over 5Pd/SA under hydrogen pressures ranging from 0.7 MPa to 10.3 MPa, the yield of **1** increased from 8% to 39%. The increased pressure serves to maintain the Pd centers in a reduced state and covered with activated hydrogen. The high hydrogen pressure needed for this conversion may explain why the preparation of **1** from xylose has not been reported previously.

2.3.2. Effect of Pd loading

The palladium catalysts were prepared at nominal palladium loadings of 3, 4, 5, and 10 wt%. Yields of **1** were not substantially affected by increasing the loading of Pd presumably due to the fact that dispersion was so low that additional Pd was lost in the inaccessible centers of the large crystallites. 3Pd/SA gave **1** in yields similar to 5Pd/SA but reactions rates were slower.

2.3.3. Effect of xylose charge

Hydrogenations were typically performed on 5% xylose solutions. However, since the formation of **1** is a dimerization, it was expected that using higher concentration xylose solutions would result in higher yields. Therefore, xylose concentrations ranging from 2 to 30% were tried. Despite expectations that higher xylose concentrations would increase yields of **1**, quite the opposite occurred. The most dilute xylose solutions gave **1** at 41% yield and this value fell to 5% from 30% solutions.

2.3.4. Reuse of the catalyst

Silica-alumina is a mesoporous oxide commonly used as a catalyst support. The well known drawback to oxide supports is their degradation in hot water resulting in loss of surface features and often loss of supported precious metals [32]. As is shown in Table 1, the catalysts were affected by the reaction conditions resulting in catalysts of considerably lower surface area and slightly increased pore volume with pores about twice as large as the starting materials. However, these changes had little effect on catalyst performance after two runs. Fig. 3 shows the product distribution over three catalytic runs using 10 wt% xylose solutions. Following each run, the catalyst was collected, washed, and recalcined to remove any coke deposits. Included on the bar graph are points indicating the conversion and carbon balance for each run. Conversion in the third run remained high but the carbon balance fell from 83% to 76%. This suggests that xylose or products are being lost to higher molecular weight species perhaps resulting from oligomerization.

2.3.5. Hydrodeoxygenation of ribose, L-arabinose, and xylooligosaccharides

L-Arabinose is the other pentose commonly found in hemicellulose and successful conversion of this sugar would allow for the direct use of xylan. Indeed, the HDO of L-arabinose gave the same product selectivity as did the HDO of xylose. Unfortunately, this comparison sheds no light on a possible reaction mechanism. L-Arabinose is considerably more stable in hot water than is xylose, whether in the presence of mild Brønsted acid [29] or the Lewis acid catalyst $FeCl_3$ [6]. If the reaction were running through furfural, higher yields would be expected from xylose since it dehydrates faster than does L-arabinose. If the reaction were running through the ketopentoses xylulose or ribulose, higher yields would be expected from arabinose since its greater stability would allow for conversion to these intermediates. D-Ribose also gave the same product distribution from its HDO over 5%Pd/SA. These results are presented in Fig. 4. Each of the substrates was subjected to HDO using the 5%Pd/SA catalyst at 433 K and 7 MPa H_2 pressure and the reaction time was 5.5 h for each.

A mixture of xylooligosaccharides was also subjected to HDO using the 5%Pd/SA catalyst at 160 °C and 7 MPa H_2 pressure but at a lower substrate concentration of 2 wt% rather than the 5 wt% of the monosaccharide reactions. This reaction produced **1** at a selectivity of 31% which is about the same as that from the monosaccharides. However, the selectivity toward xylitol was almost double that of what was formed from xylose, and the production of the hydrogenolysis products was considerably lower. The production of **1** at yields similar to that obtained from the pentoses indicates that the catalyst is able to hydrolyze oligosaccharides. However, efforts to get beechwood xylan to hydrolyze and produce **1** failed, presumably due to the inaccessibility of the xyl-xyl linkages in the polymer to the heterogeneous catalyst.

2.3.6. Crystal structure of *1*

X-ray quality crystals of compound **1** were obtained by slow evaporation of an ethyl acetate solution of the compound. The crystallography decisively establishes the stereochemistry of **1** to be the *meso* diastereomer of 1,6,9,13-tetraoxadispiro(4.2.4.2)tetradecane. Initially data were collected at 100 K on two separate crystals, and both were found to be an apparently different polymorph than the established room temperature structure of **1** reported by Gaede [26]. Therefore, data on a third crystal were collected at 298 K, and unlike the triclinic low temperature structures, these data were consistent with a monoclinic polymorph indistinguishable from the structure reported by Gaede. To clarify whether the polymorphism was the result of crystallization of distinct crystal forms, or the result of a temperature dependent solid state phase transition, a separate crystal was selected and diffraction data on the crystal were collected at seven different temperatures. The first data set was collected at 273 K then with the crystal remaining on the instrument, the temperature was lowered as five successive data sets were collected down to 100 K. To demonstrate the reversibility of the temperature effects, the crystal was warmed to 260 K while

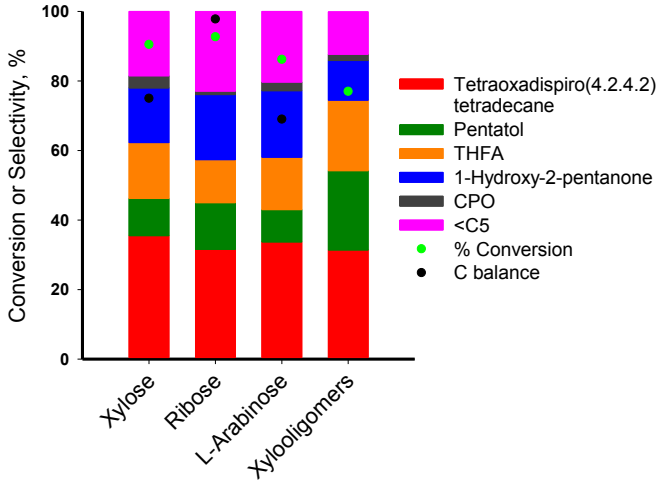

Fig. 4. Product selectivity resulting from the hydrodeoxygenation of pentoses and xylooligomers over 5%Pd/SA. Conditions are described in the text.

remaining on the instrument and a seventh and final data set was collected. Key experimental data parameters for the variable temperature study are shown in Table S3. At 273 K and 220 K, the crystal retained its monoclinic form with compound **1** centered on a crystallographic inversion center, with half of the molecules atomic coordinates being symmetry generated. By 175 K, the crystal had undergone a phase transition to a triclinic form with two crystallographically independent molecules in the unit cell, each centered on a crystallographic inversion center, with half of each molecule's atomic coordinates being symmetry generated. Upon close examination, this is much less profound than it may initially sound. Decent in symmetry from the monoclinic $P2_1/c$ space group to a triclinic space group necessarily eliminated the glide planes that had rendered all molecules symmetry equivalent. Fig. 5a overlay of the two crystallographically independent molecules of the 100 K structure illustrate there are negligible differences in the conformations of these molecules. Furthermore, Fig. 5b overlay of a 100 K molecule with a 273 K molecule demonstrates that the conformation of these molecules are essentially equivalent.

Fig. 6 shows an ORTEP view of the central molecule in the unit cell at each temperature. While the standard uncertainty ellipses sharpen as the temperature drops, the solid state molecular conformation remains essentially static over a wide 173 K temperature range and even across a formal solid state phase change. Technically, because at lower temperatures, the crystal system has changed from monoclinic to triclinic, there is a measurable change in the solid crystalline phase and this makes detectable slight differences in the molecular (not conformational) arrangements of the molecules in the two phases. In a perspective on how to define polymorphism, Desiraju discusses several solid form examples that technically could be classified as polymorphs according to the definitions accepted since the 1960's; however, he poses the question: “but do these structures qualify for the polymorph label, in spirit?” [33] In the case of the crystal forms of **1** reported here, the answer is clearly no; for chemical purposes these crystal forms do not qualify as polymorphs. Best practices for modern X-ray crystallography demands low temperature data collection, generally below 150 K, unless there is a compelling reason to collect data at a higher temperature. Less than a decade ago, room temperature data collection was routine. As more structures, originally measured at room temperature, are re-determined at low temperature, inevitably some will be found to have ‘different’ crystal forms at low temperature. The variable temperature structures of **1** provide an important and tangible example where an observed difference in crystal form may not be evidence for polymorphism, beyond the most rigorous and narrow of definitions. They also provide a reminder that care must be taken when comparing crystallographic results between crystals not measured under identical data collection conditions, particularly when the differences in results might, as was the case here, be attributable simply to the differences in data collection conditions. (The X-ray experimental parameters for the variable temperature structures are in the SI.)

2.4. Reactions of *1*

2.4.1. Ring opening over Amberlyst 15 and acetylation

Though **1** could find uses as a fragrance, we sought to expand its potential as a biobased material. To this end, we have demonstrated the ring-opening of **1** to the linear form, followed by esterification of the two resulting alcohol groups. The solid acid Amberlyst 15 was shown to open the ring structure of **1** in aqueous solutions. The product of this reaction is 1,5-dihydroxy-2-pentanone, **3**. The intermediate monomeric species, **2**, is not detected in these solutions and has only been isolated in acetone during flash chromatography purification. Once **3** is formed, it can be esterified at each of the alcohol groups using vinyl acetate in phosphate buffer. This gives 1,5-bis(acetyloxy)-2-pentanone, **4**. This compound was identified by Zhang et al. as being an inhibitor of human and mouse 11β-hydroxysteroid dehydrogenases [27]. The acetylated compound should also be amenable to further chemistry such as transesterification to give new biobased materials.

3. Conclusions

D-(+)-xylose, D-(−)-ribose, and L-arabinose can be hydrodeoxygenated to 1,6,9,13-tetraoxadispiro(4.2.4.2)tetradecane in water using Pd/SA as catalyst in about 40% yield. The product can be isolated using solid phase and liquid-liquid extractions. In its crystal form, **1** undergoes a phase change from triclinic to monoclinic between 175 K and 225 K, though this change is strictly molecular rearrangement and not polymorphism. This tricyclic compound can be ring-opened by solid acid catalysts and the resulting diol can then be esterified to give 1,5-bis(acetyloxy)-2-pentanone. Though the silica-alumina support is degraded by the hot water reaction conditions used here, it can still be reused with little loss of selectivity.

4. Experimental

4.1. Materials and methods

$PdCl_2$, silica-alumina, D-(−)-ribose, L-arabinose, vinyl acetate, and Amberlyst 15 were from Sigma-Aldrich (Milwaukee, WI, USA). D-(+)-Xylose was from Alfa Aesar (Ward Hill, MA, USA). Xylooligosaccharides were from Wako (Osaka, Japan) and described as a mixture of xylobiose, xylotriose, etc.

4.2. Catalyst preparation and characterization

The palladium catalysts were prepared by wet impregnation. $PdCl_2$ was dissolved in 9%NH_4OH and the resulting solution was

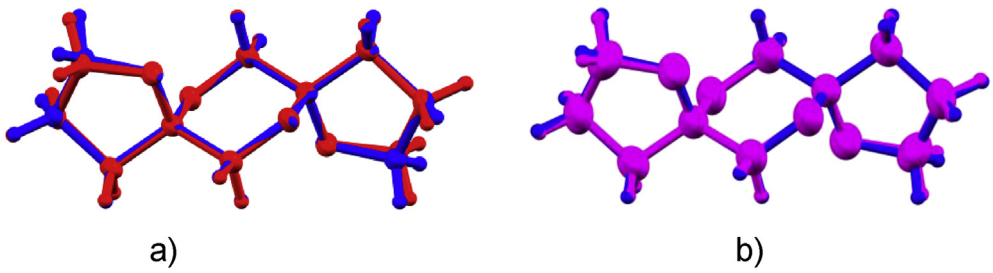

Fig. 5. Overlays of a) crystallographically independent molecules at 100 K (red and blue) and b) molecules at 100 K (magenta) and 273 K (blue). (For interpretation of the references to colour in this figure legend, the reader is referred to the web version of this article.)

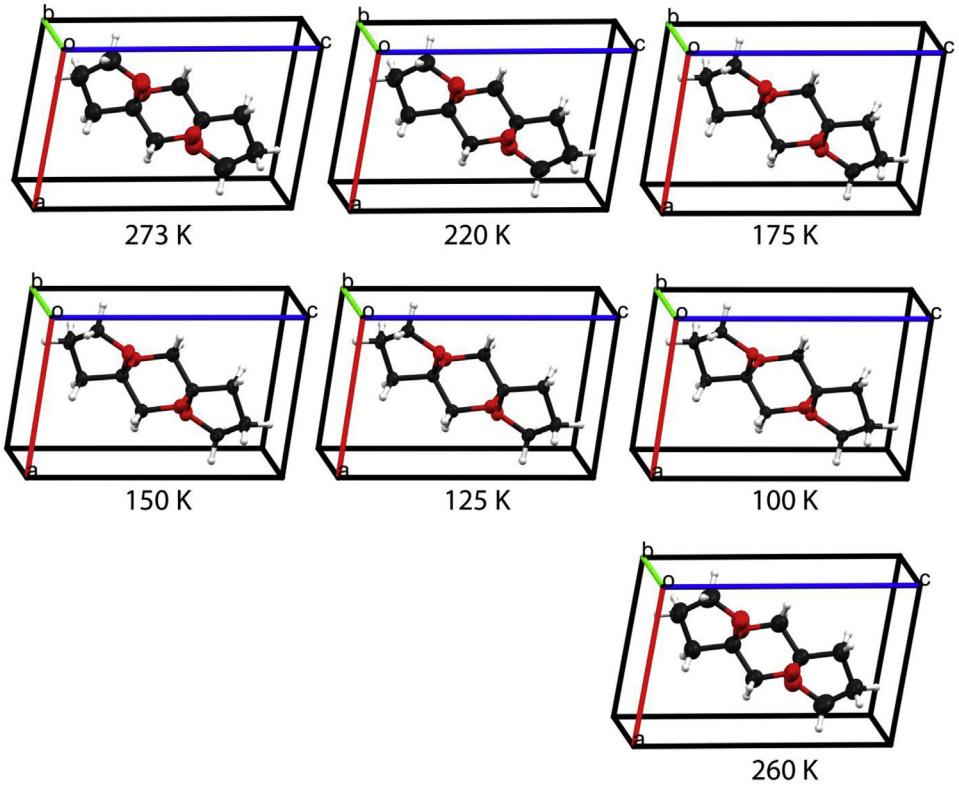

Fig. 6. Color Mercury generated, POV-Ray rendered ORTEP drawing (50% probability level, hydrogen atoms drawn arbitrarily small) of compound **1** at various temperatures.

stirred into the appropriate mass of silica-alumina to give a damp mixture. This was air-dried and then calcined in static air at 673–973 K for 2 h. Surface textures were determined using a Quantachrome ASiQ (Quantachrome Instruments, Boynton Beach, FL, USA). Samples were outgassed at 200 °C for 10 h prior to analysis. Analyses were performed at 77 K using N_2 as the adsorptive. Surface areas were determined using the BET equation within $0.05 < P/P_o < 0.30$. Pore sizes were determined using the BJH method on the adsorption branch of the isotherms. Energy Dispersive Spectroscopy (EDS) measurements were made on a JOEL JSM-6010LA SEM with an integrated EDS attachment operating at 10 keV. X-ray diffractograms were recorded on a Bruker D2 Phaser (Bruker AXS Inc., Billerica, MA) using θ/θ geometry and Cu-Kα radiation generated at a current of 10 mA and 30 kV. Scans were run over a 2θ range of 10–90° with a step size of 0.02° and a time per step of 0.2 s. The sample stage was rotated at 10 rpm during the scan. Initial divergence slit size was 0.6 mm and a 1 mm air scatter screen was used above the sample. A Lynxeye™ detector was used in conjunction with a 2.5° Soller slit and a Ni Kα filter.

4.3. Analytical methods

Generally, HPLC analyses were performed on a Carbomix column maintained at 323 K using 0.025 M H_2SO_4 as mobile phase. Analytes were measured using a Finnigan Surveyor refractive index detector. Separation of the ribose/ribitol mixes was accomplished using an ion moderated partition chromatography column (Aminex HPX-87P with deashing and Carbo-P micro-guard cartridge from Bio-Rad Laboratories Inc., Hercules, CA). The column was maintained at 353 K, and the samples were eluted with Milli-Q filtered water at a flow rate of 0.6 ml/min. All solutes were identified and quantified by comparison to retention times of authentic standards.

GCMS Analyses were performed on a Shimadzu QP2010 SE GC/mass spectrometer/FID. Separations were accomplished using a Supelco Petrocol DH 50.2 (50 m × 0.2 mm × 0.5 μm) column. The oven program was as follows: Initial temperature 348 K for 2 min, ramp at 10 °C/min to 453 K, hold for 1 min then a ramp at 25 °C/min to 548 K with a final hold time of 3 min. Methyl nonanoate was used as internal standard. The mass spectrometer was operated in the EI mode at 70 eV. Prior to GC analysis, 4.0 ml of the filtrate resulting after removal of the catalyst, were loaded onto a 5 g Hypersep C18 solid phase extraction column (Thermo Scientific, Rockwood, TN, USA). The products eluted with 8.0 ml methanol. This solution was then spiked with internal standard and analyzed. ^1H and ^{13}C NMR spectra were obtained on a Bruker Avance 500 with a 5 mm dual proton/carbon probe (500 MHz ^1H/125 MHz ^{13}C).

4.4. Synthesis of 1,6,9,13-tetraoxadispiro(4.2.4.2)tetradecane from xylose

Reactions were performed in a Parr Instruments (Parr Instruments, Moline, IL, USA) stirred reactor with a 300 ml glass liner. Typically, xylose and catalyst were loaded into the reactor with 50 ml water, the system was charged with hydrogen and evacuated five times before being brought up to 15 bar hydrogen. The reactor was then heated to 433 K and pressurized to the final hydrogen pressure and the reactor was stirred at 250 rpm until the reaction was complete. Progress of the reaction was monitored by withdrawing samples via a sampling tube and analyzing by HPLC for unreacted xylose. Upon completion of the reaction, typically after 5 h, the catalyst was removed by filtration. The filtrate was extracted with diethyl ether to remove HPO, CPO, and some of the THFA. The aqueous portion was then reduced in volume at reduced pressure to give a heavy residue. This residue was then extracted with 90:10 hexane:ethyl acetate. Removal of this solvent mix at reduced pressure gave solid **1**. ^{13}C NMR (D_2O, 125 MHz) δ22.8, 33.1,

64.6, 68.4, 103.1. ^{1}H NMR (D_2O, 500 MHz): δ1.74 (complex multiplet, 2H), 1.84 (complex multiplet, 2H), 1.9 (complex multiplet, 2H), 1.97 (complex multiplet, 2H), 3.48 (d, J = 12.5, 2H), 3.95 (t, J = 7, 2H, 4.05 (d, J = 12.5, 2H)). EIMS *m/z*, (relative intensity) 84, (100); 42 (21); 56 (16); 43 (11).

Isolation of the ring–closed monomer (**2**) was accomplished using flash chromatography (CombiFlash R_f 200i, Teledyne Isco, Lincoln, NE, USA). Separations were performed using two stacked Redi-Sep Gold Silica columns (12 g each). The mobile phase was a hexane/ethyl acetate gradient flowing at 25 ml/min. The gradient used was a 1–10 column volume (CV) gradient to 10% EtOAC, hold at 10% EtOAc for 30 CV, then up to 100% EtOAc in 10 CV, hold for 10 CV, then 0% EtOAc for 5 CV. Detection was accomplished using an electrospray detector held at 313 K.

2-hydroxy-2-hydroxymethyltetrahydrofuran, **2**. ^{13}C NMR (acetone-d_6, 125 MHz): δ 23.2, 33.6, 64.7, 67.1, 102.4. ^{1}H NMR (acetone-d_6, 500 MHz): δ1.61 (complex multiplet, 2H), 1.78 (complex multiplet, 2H), 1.85 (complex multiplet, 2H), 1.97 (complex multiplet, 2H), 2.77 (t, J = 0.8, 1H), 2.81 (s, 1H), 3.36 (d, J = H), 3.88 (m, J = 6.0, 2H), 4.01(d, J = 11.5, 2H). EIMS *m/z*, (relative intensity) 101, (100); 59, (88); 43, (28); 41, (28).

4.5. Crystallographic experimental details of **1**

X-ray quality crystals of compound **1**, $C_{10}H_{16}O_4$, were obtained by slow evaporation of an ethyl acetate solution of the compound. Several crystals ranging in size from tenths of mm to several mm were suspended in mineral oil at ambient temperature. Preliminary diffraction data was collected on three samples, including: a 100 K data set of an irregularly shaped fragment, selected from an originally several mm plate; a 100 K data set of a native plate less than 0.5 mm across; and a 298 K data set of an irregularly shaped fragment, selected from a different plate. Based on this data, it was decided that best practice would be to collect data sets at various temperatures on a single sample. A suitable mineral oil coated colorless plate with approximate dimensions 0.200 mm × 0.085 mm × 0.075 mm was selected and mounted on a 50 μm MicroMesh MiTeGen Micromount then transferred to a Bruker AXS SMART APEX CCD X-ray diffractometer. The X-ray diffraction data were collected using Mo-K_α (λ = 0.71073 Å) radiation. Seven data sets were collected on this crystal, without further adjustment to the crystal mounting (or even opening the diffractometer's hutch doors) once the first data set collection began. Data sets were collected in the order: 273(2) K, 220(2) K, 175(2) K, 150(2) K, 125(2) K, 100(2) K and 260(2) K. For each data set, a total of 1388 frames were collected. The exposure time was 3.86 h for each data set, which was 27.0 h total exposure time for the crystal. The frames were integrated with the Bruker SAINT software package using a narrow-frame algorithm [34]. The integration of the 273 K, 220 K, and 260 K data were best accomplished using monoclinic unit cells. The integration of the 175 K, 150 K, 125 K, and 100 K data were best accomplished using triclinic unit cells, and integrating each data set as pseudo-merohedral twins. While it is possible to achieve 'acceptable' refinement metrics by integrating the data as not-twinned, free refinement of the relative batch scale factors (0.3863 at 175 K, 0.3676 at 150 K, 0.3618 at 125 K, 0.3674 at 100 K) were both consistent with the observed relative batch scale factors (0.3724 at 175 K, 0.3594 at 150 K, 0.3566 at 125 K, 0.3572 at 100 K), and each other. Data were corrected for absorption effects using the multi-scan methods (SADABS for the non-twinned data and TWINABS for the twinned data) [34]. Solution and data analysis were performed using the WinGX software package [35]. The solutions were achieved by charge-flipping methods using the program SUPERFLIP [36] and the refinements were completed using the program SHELX-2016 [37]. All non-H atoms were refined anisotropically. (C–H = 0.99 Å for CH_2; U_{iso}(H) = 1.2U_{eq}(C)). Full-matrix least-squares refinements on *F* [2] led to convergence of all structures and the final difference Fourier syntheses showed all residual electron density to be within accepted norms. All residual electron density was deemed of no chemical significance. Crystal data, data collection and structure refinement details are summarized in Table S1–S3. Molecular diagrams were generated using Mercury [38]. CCDC 1458991-1458997 contain the supplementary crystallographic data for this paper. These data can be obtained free of charge from the Cambridge Crystallographic Data Centre via https://summary.ccdc.cam.ac.uk/structure-summary?ccdc=1458991-1458997.

4.6. Ring opening and acetylation of 1,6,9,13-tetraoxadispiro(4.2.4.2)tetradecane

200 mg of **1** and about 50 Amberlyst 15 beads were stirred and gently heated in 2 ml H_2O for 60 min. The Amberlyst beads were removed and the solution was poured into aqueous Na_3PO_4 buffer (pH 10; 3% w/v final) containing vinyl acetate (200 μL). After 18 h at room temperature the reaction was dried down on an airline. The residue was dissolved in pyridine (2 ml) and treated with acetic anhydride (2 ml, 313 K; 20 min). This was cooled, dried down, re-dissolved in ethyl acetate, and back-washed with water to give the final product in the organic layer. 1,5-Dihydroxy-2-pentanone (**3**). ^{13}C NMR (D_2O, 125 MHz): δ25.7, 34.6, 61.1, 67.1, 213. ^{1}H NMR (D_2O, 500 MHz): δ1.75 (p, J = 7, 2H), 2.48 (t, J = 7.5, 2H), 3.53 (t, J = 6.5, 2H), 4.32 (s, 2H). EIMS *m/z*, (relative intensity) 87, (100); 41 (70); 43 (63); 69 (32). 1,5-bis(acetyloxy)-2-pentanone (**4**). ^{13}C NMR ($CDCl_3$, 125 MHz): δ20.44, 20.87, 22.30, 35.17, 63.32, 67.90, 170.22, 170.98, 202.86. ^{1}H NMR ($CDCl_3$, 500 MHz): δ1.97 (p, J = 6.5, 2H), 2.06 (s, 3H), 2.18 (s, 3H), 2.52 (t, J = 7.0, 2H), 4.1 (t, J = 6.0, 2H), 4.68 (s, 2H). EIMS *m/z*, (relative intensity) 43, (100); 87 (69); 129 (16); 42 (7).

Acknowledgements

The assistance of Trina Hartmann in the conversion of 1,6,9,13-tetraoxadispiro(4.2.4.2)tetradecane to 1,5-bis(acetyloxy)-2-pentanone is greatly appreciated, Mr. Greg Kennedy for the ribitol/ribose separations, and Dr. Arthur Thompson for performing the EDS analyses. The authors thank NSF-CHE (grant #1039689) for funding the X-ray diffractometer.

Appendix A. Supplementary data

Supplementary data related to this article can be found at http://dx.doi.org/10.1016/j.carres.2016.06.003.

References

[1] J.-P. Mikkola, H. Vainio, T. Salmi, R. Sjöholm, T. Ollonqvist, J. Väyrynen, Appl. Catal. A Gen. 196 (2000) 143–155.
[2] M. Yadav, D.K. Mishra, J.-S. Hwang, Appl. Catal. A Gen. 425–426 (2012) 110–116.
[3] reportbuyer.com,August 27, 2014, http://www.prnewswire.com/news-releases/xylitol--a-global-market-overview-272903331.html.
[4] J.B. Binder, J.J. Blank, A.V. Cefali, R.T. Raines, ChemSusChem 3 (2010) 1268–1272.
[5] M.B. Fusaro, V. Chagnault, D. Postel, Carbohydr. Res. 409 (2015) 9–19.
[6] S.L. Guenic, F. Delbecq, C. Ceballos, C. Len, J. Mol. Catal. A Chem. 410 (2015) 1–7.
[7] X. Hu, R.J.M. Westerhof, D. Dong, L. Wu, C.-Z. Li, ACS Sustain. Chem. Eng. 2 (2014) 2562–2575.
[8] P.K. Khatri, N. Karanwal, S. Kaul, S.L. Jain, Tetrahedron Lett. 56 (2015) 1203–1206.
[9] K. Lamminpää, J. Ahola, J. Tanskanen, Bioresour. Technol. 177 (2015) 94–101.
[10] I. Sádaba, S. Lima, A.A. Valente, M. López Granados, Carbohydr. Res. 346 (2011) 2785–2791.

[11] J. Zhang, J. Zhuang, L. Lin, S. Liu, Z. Zhang, Biomass Bioenergy 39 (2012) 73–77.
[12] L. Zhang, H. Yu, P. Wang, Y. Li, Bioresour. Technol. 151 (2014) 355–360.
[13] N.S. Biradar, A.M. Hengne, S.N. Birajdar, P.S. Niphadkar, P.N. Joshi, C.V. Rode, ACS Sustain. Chem. Eng. 2 (2014) 272–281.
[14] F. Dong, Y. Zhu, H. Zheng, Y. Zhu, X. Li, Y. Li, J. Mol. Catal. A Chem. 398 (2015) 140–148.
[15] M. Lesiak, M. Binczarski, S. Karski, W. Maniukiewicz, J. Rogowski, E. Szubiakiewicz, J. Berlowska, P. Dziugan, I. Witońska, J. Mol. Catal. A Chem. 395 (2014) 337–348.
[16] Y. Nakagawa, K. Takada, M. Tamura, K. Tomishige, ACS Catal. 4 (2014) 2718–2726.
[17] P. Panagiotopoulou, D.G. Vlachos, Appl. Catal. A Gen. 480 (2014) 17–24.
[18] S. Sitthisa, T. Sooknoi, Y. Ma, P.B. Balbuena, D.E. Resasco, J. Catal. 277 (2011) 1–13.
[19] S. Kim, M.K. Mayeda, E. Sasmaz, J. Lauterbach, ACS Sustain. Chem. Eng. 3 (2015) 381–385.
[20] S. Liu, Y. Amada, M. Tamura, Y. Nakagawa, K. Tomishige, Green Chem. 16 (2014) 617–626.
[21] S. Liu, Y. Amada, M. Tamura, Y. Nakagawa, K. Tomishige, Catal. Sci. Technol. 4 (2014) 2535–2549.
[22] Y. Nakagawa, K. Tomishige, Catal. Today 195 (2012) 136–143.
[23] F. van der Klis, L. Gootjes, J. van Haveren, D.S. van Es, J.H. Bitter, Green Chem. 17 (2015) 3900–3909.
[24] C.D. Hurd, O.E. Edwards, J. Org. Chem. 14 (1949) 680–691.
[25] S. Swadesh, A.P. Dunlop, J. Org. Chem. 14 (1949) 692–695.
[26] B. Gaede, R. Henry, S.A. Chamberlin, J. Heterocycl. Chem. 37 (2000) 1333–1335.
[27] L. Zhang, Y. Shen, H.-J. Zhu, F. Wang, Y. Leng, J.-K. Liu, J. Antibiot. 62 (2009) 239–242.
[28] B.S. Hamilton, F. Himmelsbach, H. Nar, A. Schuler-Metz, P. Krosky, J. Guo, R. Guo, S. Meng, Y. Zhao, D.S. Lala, L. Zhuang, D.A. Claremon, G.M. McGeehan, Eur. J. Pharmacol. 746 (2015) 50–55.
[29] B. Danon, W. Hongsiri, L. van der Aa, W. de Jong, Biomass Bioenergy 66 (2014) 364–370.
[30] R. Fang, H. Liu, R. Luque, Y. Li, Green Chem. 17 (2015) 4183–4188.
[31] J. Guo, G. Xu, Z. Han, Y. Zhang, Y. Fu, Q. Guo, ACS Sustain. Chem. Eng. 2 (2014) 2259–2266.
[32] R.M. Ravenelle, J.R. Copeland, W.-G. Kim, J.C. Crittenden, C. Sievers, ACS Catal. 1 (2011) 552–561.
[33] G.R. Desiraju, Cryst. Growth Des. 8 (2008) 3–5.
[34] Bruker AXS Inc., Madison, WI, USA 2013.
[35] L.J. Farrugia, J. Appl. Crystallogr. 45 (2012) 849–854.
[36] L. Palatinus, G. Chapuis, J. Appl. Crystallogr. 40 (2007) 786–790.
[37] G. Sheldrick, Acta Crystallogr. Sect. C 71 (2015) 3–8.
[38] C.F. Macrae, I.J. Bruno, J.A. Chisholm, P.R. Edgington, P. McCabe, E. Pidcock, L. Rodriguez-Monge, R. Taylor, J. van de Streek, P.A. Wood, J. Appl. Crystallogr. 41 (2008) 466–470.